Sonochemical Activation of Al/Ni Hydrogenation Catalyst

Jana Dulle, Silke Nemeth, Ekaterina V. Skorb, Torsten Irrgang, Jürgen Senker, Rhett Kempe, Andreas Fery, and Daria V. Andreeva**

This paper proposes a sonochemical approach to the nanostructuring of Al/Ni catalyst with high content of accessible Ni centers and a high reusability. The surface and bulk composition as well as pore size distribution of this catalyst are controlled synergistically by adjusting the ultrasound intensity in aqueous solution. Sonochemical activation of Al/Ni alloy leads to formation of mesoporous Al/Ni metallic based frameworks with surface area up to 125 $m^2 g^{-1}$, and regular distribution of nickel active center in the porous matrix. One of the opportunities of porous Al/Ni catalyst is that due to a time-resolved controllable formation of protective oxide layer it can be stored and handled under air in comparison to traditional Raney catalysts which need inert conditions. The Al/Ni catalyst is characterized by scanning electron microscopy (SEM), electron diffraction spectroscopy (EDS), X-ray photoelectron spectroscopy (XPS), confocal scanning fluorescence microscopy (CSFM), solid-state NMR experiments, and powder X-ray diffraction analysis (PXRD). The catalytic activity was investigated for the hydrogenation of acetophenone.

1. Introduction

In recent years attention has been devoted to nanostructured metals because of their unique properties and potential applications in a variety of fields.[1–5] Especially their use as a support material and/or active agent for heterogeneous catalyst became more important.[6–8] Approaches towards the fabrication of porous metals are based on both template-free and template-assisted methods. Typical template-free methods are chemical or electrochemical dealloying procedures.[9] Mesoporous gold, platinum, and palladium can be formed by the dealloying process.[10] The formation of a uniform porosity after the dealloying process is possible if an alloy system is a monolithic phase because the nanoporosity is formed by a self-assembly process through surface diffusion and not by the simple dissolution of one phase from a multiphase system. For example, mesoporous gold prepared by dealloying from gold–silver alloys has disordered mesostructures, and the wide pore-size distributions of these mesostructures are not suited for the selective transport and adsorption of catalyzed species. A typical example of chemical dealloying is the preparation of "Raney nickel".[11] Raney nickel is produced when a block of a nickel-aluminum alloy is treated with concentrated sodium hydroxide. However, the dissolution of aluminum ions during the catalyst formation step could accelerate the formation of catalytically inactive surface nickel aluminate species.

The template methods are based on electroplating,[12] chemical reduction,[13] or plasma spraying[14] techniques. These methods require the use of preformed templates, such as self-assembled liquid-crystal surfactants,[15] colloidal crystals,[16] porous block copolymers,[17] or anodic porous alumina.[18] By using mesoporous silica as a template, mesoporous metals with highly ordered networks and a narrow pore-size distribution can be obtained. Because fluoric acid or sodium hydroxide is used to remove silica, the metals prepared using this method are limited to those unaffected by the dissolution agents (e.g. gold, platinum, and silver).[19] The template methods also have some disadvantages. These methods are multistage and involve a sacrificial second phase, which increases production costs because of the formation of the template and its subsequent removal, combined with the waste generation, especially when up-scaling the procedure.

Supported nickel catalysts play an important role in heterogeneous catalysis such as hydrogenation, hydrogenolysis, and partial oxidation of methane. One of the most successful methods of the activation of Al/Ni systems is the so-called Raney process, patented by the American engineer Murray Raney in 1925.[11,20] This process based on oxidation of aluminum to aluminum oxide and partial dissolution of aluminum component by using a strong base solution. However, the hydrolysis rate of alumina

J. Dulle, S. Nemeth, Prof. A. Fery, Dr. D. V. Andreeva
Chair of Physical Chemistry II
University of Bayreuth
Universitätsstr. 30, Bayreuth 95440, Germany
E-mail: daria.andreeva@uni-bayreuth.de
Dr. T. Irrgang, Prof. R. Kempe
Inorganic Chemistry II
University of Bayreuth
Universitätstr. 30, Bayreuth 95440, Germany
E-mail: kempe@uni-bayreuth.de
Dr. E. V. Skorb
Max Planck Institute of Colloids and Interfaces
Wissenschaftspark Golm
Am Mühlenberg 1, Golm 14476 Germany
Prof. J. Senker
Inorganic Chemistry III
University of Bayreuth
Universitätsstr. 30, Bayreuth 95440, Germany

DOI: 10.1002/adfm.201200437

precursor in Raney process is difficult to control. The final outcome is pyrophoric and sensitive to storage conditions.[21,22] These facts encouraged us to apply an ultrasound of high intensity (USHI) for the activation of the Al/Ni alloy, where the output is a catalytic active Al/Ni catalyst, which can be stored and handled under ambient conditions.

Recently[23–28] we have found that ultrasound treatment had dramatic effects on the morphology of aluminum particles. In particular, surface areas of the sonicated colloidal particles could be significantly increased when compared with untreated colloids. Intensive etching and oxidation of aluminum by ultrasound leads to formation of a sponge-like metal matrix stabilized by a thin metal oxide layer.[25] These metal sponges could be a perfect support for a heterogeneous catalyst. Based on the known physical and chemical effects of the high-intensity ultrasound outlined in Ref. [23–39] we expect that properties of metals such as resistance to oxidation and melting point could determine their behavior in the ultrasonic field and the final surface morphology, composition and properties of a catalyst. The dramatically different ability of the metals to respond to ultrasound irradiation can be exploited for the formation of nanoscale composites; thus, if alloy particles consisting of resistant and sponge-forming compounds are treated, a microphase separation could be expected under ultrasound irradiation. We tested this idea for the aluminum/nickel (1:1) system and generated an Al/Ni alloy catalyst stabilized by a thin oxide layer. Herein, we present the results of the catalyst characterization of the sonochemically prepared/activated Al/Ni alloy powder and its application for the hydrogenation of acetophenone as a model reaction.

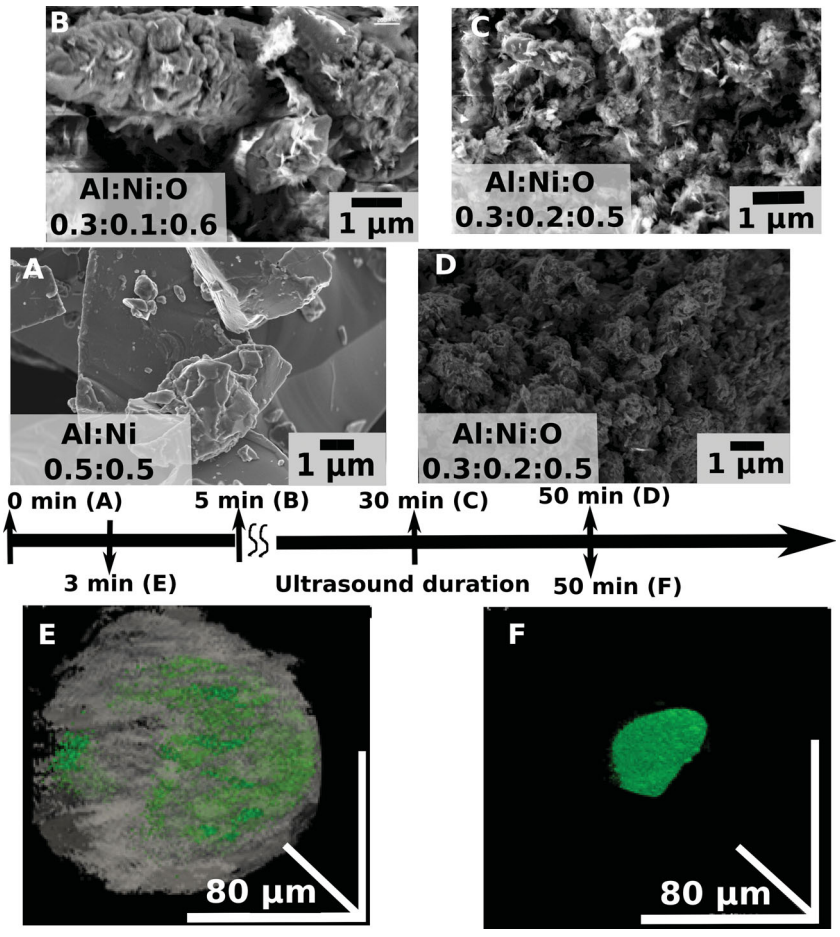

Figure 1. SEM images and the aluminum (Al), nickel (Ni) and oxygen (O) ratio measured by EDS (inserts) of Al/Ni particles: A–initial; B–after 5 min; C–30 min and D–50 min of sonication at 140 W cm^{-2}. 3D confocal microscopy reconstruction of the Al/Ni nanostructure loaded with fluorescein: (E) the alloy particle after 3 min (the reconstruction of both transmission and fluorescent mode) and (F) 50 min of sonochemicalexposure at 140 W cm^{-2}.

2. Results and Discussions

2.1. Catalyst Activation and Characterization

The sonochemical nanostructuring of metal alloys is based on microphase separation in an alloy due to different phase response to ultrasonic effects. The initial 1:1 Al/Ni alloy consists of Al_3Ni_2 and Al_3Ni intermetallides. Collapse of cavitation bubbles generated by ultrasound is followed by high local (μm^2 area) temperature (up to 5000 K) and a high heating/cooling rate. Thus, ultrasound of high intensity (USHI) provides unique conditions for metal treatment and should affect the microstructure of an alloy. Moreover, recently it was shown that aluminum could be not just oxidized itself during ultrasonic treatment in aqueous solution, but also could serve as an effective donor of reducing agent (H_2).[40] The finding is extremely important for Al/Ni catalysts in situ activation during preparation. The catalyst activation in H_2 could be expected during the catalyst formation without the total transformation of metallic nickel to oxide. We could expect even reduction process during sonication,[40] also in the porous metal matrix. The aluminum/nickel (1:1) alloy powder was treated in a 10 wt% aqueous suspension with USHI at 140 W cm^{-2} from 30 sec to 50 min. The USHI driven interparticle collisions result in continuous breakage of 100 µm initial particles. It was shown that at surfaces several times larger than the resonance cavity size (e.g., at 20 kHz the maximum size of a cavitation bubble is approximately 5 µm)[41a] microjets of liquid can impact the solid surface.[41b] Thus, we choose 100 µm initial particles in order to maximise this effect of cavitation. The scanning electron microscopy (SEM) images show that after 50 min of sonication the particles were broken into 10–20 µm species (**Figure 1**, A–D).

The 3D reconstructions of the transmission and fluorescence images of the confocal scanning fluorescence microscopy (CSFM) of the sonicated Al/Ni particles loaded with the dye demonstrate the formation of porous inner structure. As longer sonication time of the particles as deeper the dye could

DOI: 10.1002/adfm.201200437

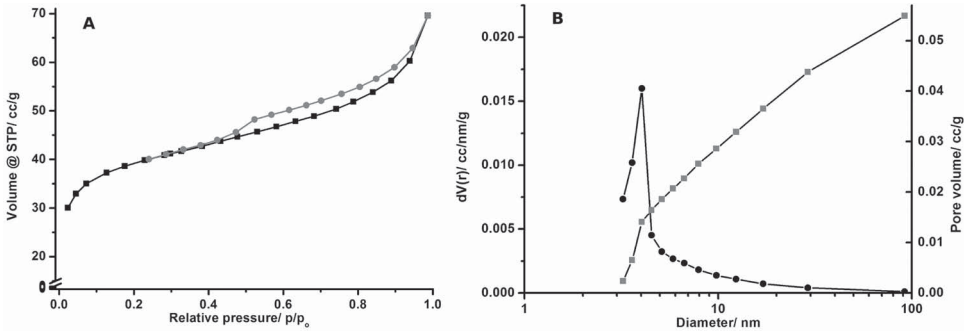

Figure 2. N_2 Adsorption (-■-)–desorption (-●-) isotherms of Al/Ni particles prepared by 50 min of sonication at 140 W cm^{-2} (A). BJH pore size distribution (-●-) and pore volume (-■-) of the same particles (B).

penetrate into the matrix of the alloy particle (Figure 1, E/F). The 50-min-sonicated samples could be completely saturated by the dye. The detailed evaluation of porous structure was made by the Barrett–Joyner–Halenda method (BJH) and the Brunauer–Emmett–Teller method (BET).[42,43] The N_2 adsorption/desorption isotherm (**Figure 2**, A) can be classified as group IIb if the new classification system proposed by Rouquerol et al.[44,45] is considered. The hysteresis loop corresponds to type H-1, according to IUPAC classification standards.[46] The pore size distribution, evaluated by BJH, proves the formation of mesopores with a pore size of about 4 nm for the Al/Ni alloy (Figure 2, B). The highest surface area according to BET was found to be 125 m^2 g^{-1} after 50 min of sonication at 140 W cm^{-2}. Initial Al/Ni alloy particles show a surface area of 0.2 m^2 g^{-1} only. We increased by a factor of 625 the surface area for our modified samples. Compared to commercial Raney nickel, which has a surface area of 50 m^2 g^{-1},[47] the sonochemically formed Al/Ni with a surface area of 125 m^2 g^{-1} exhibits a clear advantage.

In order to estimate the concentration of high-energy kinks and breaks accessible for catalysis, we analyzed the metal surface area of the Al/Ni alloys via pulse titration. For the Al/Ni material we obtained 1.14 m^2 g^{-1} metal surface of nickel, which gives a surface area per gram of nickel of 3.78 m^2 g^{-1}.

The oxidation/reduction processes during sonication were monitored by the electron diffraction spectroscopy (EDS) (Figure 1, A–D, inserts). We observed increase of oxygen concentration on metal surface which indicates oxidation process and formation of a novel metal oxide layer on the increased surface area of the porous metal matrix. The thickness of the metal oxide sonochemically generated on the surface of the modified metal was previously estimated by field ion microscopy less than 2 nm.[25]

Having in mind that the catalytic properties of a material depend on its inner structure, morphology, and composition, a closer look to the sonochemically induced changes inside Al/Ni particles has been taken. The inductively coupled plasma mass spectrometry (ICP) method showed that the overall Al:Ni ratio in the samples did not change. For the sonicated Al/Ni alloy we determined a Ni content of 49.5% before and after ultrasonic treatment. Thus, treatment does not cause leakage of active metals from the samples.

The precise analysis of the powder X-ray diffraction (PXRD) of the sonicated Al/Ni alloy in comparison to the untreated alloy shows the formation of bayerite ($Al(OH)_3$) as a main oxidation product of the aluminum (**Figure 3**, A/C). The initial Al/Ni alloy consists mostly of intermetallic Al_3Ni_2 with an admixture of Al_3Ni. Upon USHI treatment, bayerite appears as the main oxidation product, while the relative concentration of Al_3Ni_2 exhibits the most pronounced decrease (the Al_3Ni phase remains untouched). Nickel metal is not evident in diffraction pattern. Although in an oxide form, nickel would be rather crystalline than amorphous. The absence of the characteristic patterns of NiO might be explained its low concentration in

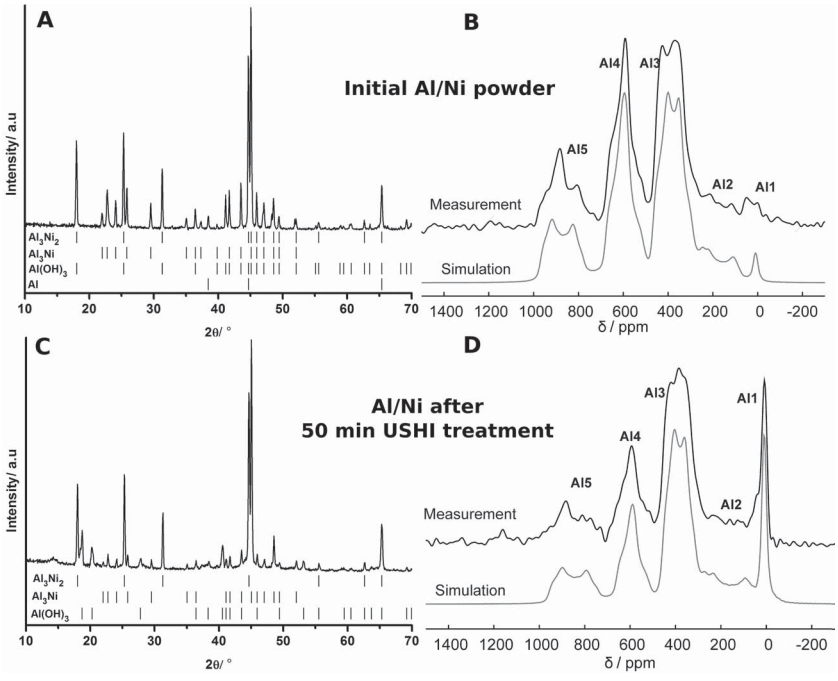

Figure 3. PXRD (left) and ^{27}Al NMR (right) of Al/Ni -alloy particles: initial (A/B) and after 50 min of sonication at 140 W cm^{-2} (C/D). 27AlNMR spectra were recorded by using $[Al(H_2O)_6]^{3+}$ as a reference. (*) indicates the spinning sidebands.

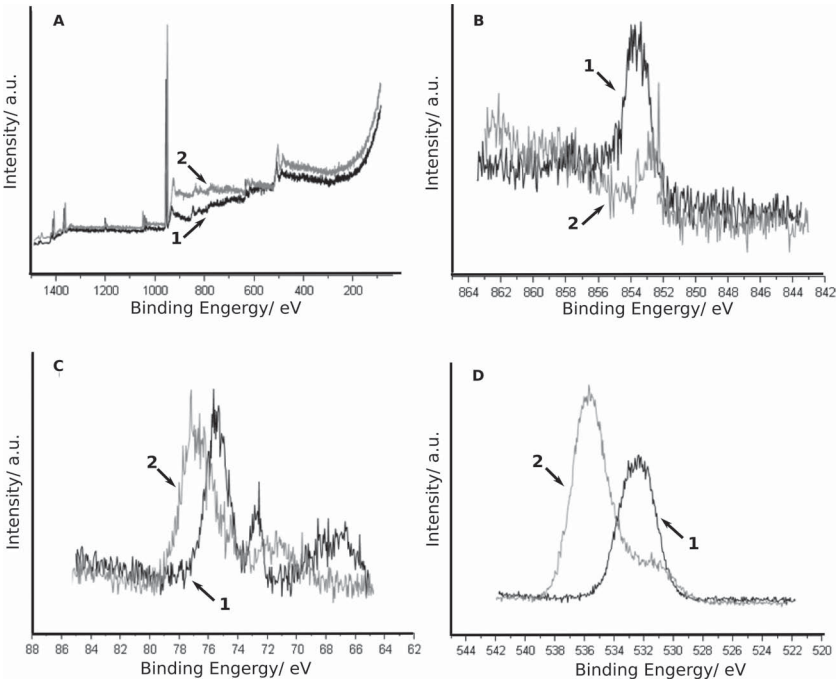

Figure 4. X-ray photoelectron (XPS) spectra of samples before (1) and after 50 min (2) of sonication treatment at 140 W cm^{-2} intensity. Survey spectra (A), Ni2p peaks (B), Al2p peaks (C), and O1s peaks (D).

the system also due to its in situ reduction by hydrogen produced in sonogenerated pores. Nickel oxide was not detected probably due to mentioned reduction process and its negligible quantity per surface area. Nickel being amorphous also does not show pronounced peak in PXRD. Thus, beside cavitation induced oxidation process, we can expect the continuous reduction of the nickel particles due to formation of reducing agent (hydrogen).[40] We propose that ultrasound-driven activation of Al/Ni particles results in the formation of a Al/Ni mesoporous matrix stabilized by a thin oxide layer. In situ activated nickel centers by partial reduction of nickel particles are probably distributed in porous matrix (see also the TEM image in Figure S1). In order to prove this consideration we performed the detailed nuclear magnetic resonance (NMR) and X-ray photoelectron spectroscopy (XPS) analysis of the novel material.

Solid state ^{27}Al NMR experiments proved presence of metallic and oxidized aluminum species. Due to the quadrupolar interaction the ^{27}Al NMR resonances are usually broad and structured. Nevertheless, at least five different species can be distinguished. The sharp resonance at 10 ppm (Al1) appears significantly only in the spectrum of the sonicated sample, which can be assigned to aluminum oxide or hydroxide (Figure 3, B/D). All other four resonances (Al2-Al5 with $\sigma_{iso} \approx$ 300 ppm, 470 ppm, 670 ppm, and 980 ppm) are dominated by both the knight shift and the quadrupolar interaction, which demonstrates that they belong to different Al/Ni alloys with a low local symmetry for the Al sites. Details of the relevant refinement parameters are given in supporting information. The ^{27}Al MAS NMR spectra show that the metal particles are composed of the same alloy phases before and after the sonication. Although the intensities of the ^{27}Al resonances might be hampered by different spin-spin relaxation times, the comparison between both data sets reveals that mainly alloy phase Al4 is affected during the sonication process.

The XPS analysis is demonstrated in **Figure 4**. The spectra were recorded before and after 50 min of ultrasonic treatment of the particles at 140 W cm^{-2}. The components at 852.3 (shown in Figure 4, B) and 854.0 can be attributed to metallic Ni and NiO.[48,49] Peaks position indicates the partial reduction of Ni during the process. After 5-min-sonication we could observe in the spectra the peaks related to the metal oxides only. However after 50-min-sonication we could distinguish the peaks of metallic nickel in the XPS patterns. The fact of formation of metallic nickel could be explained due to in situ activation of catalyst centers (Ni) during sonication. Aluminum peaks can be attributed to both phases: metallic aluminum and the oxidized aluminum. The peaks of aluminum and nickel oxides indicate partial surface oxidation (see also PXRD (Figure3)) of metals in the alloy. Thus, we can conclude that the sonochemical activation of the Ni/Al catalyst is probable due to generation of H_2[40] during partial oxidation of aluminum matrix. A conceptual novelty of the proposed ultrasound assisted Al/Ni activation is redox reactions controllable by sonication parameters and the material itself. The structure optimization for maximum catalytic efficiency can be done by adjustment of time and intensity of solication and catalyst composition.

By summarizing the results illustrated in Figures, we see that: (i) at the beginning stages of sonication of the alloy particles the increase of oxide phase could be attributed to partial oxidation of aluminum and nickel and the formation of porous structure with increased surface area; (ii) further sonication results in generation of metallic Ni detected by XPS due to possible reduction process[40] in porous matrix. Thus, relaying on the analytical methods we can assume that the sonochemically activated Al/Ni catalyst composed on unmodified Al/Ni skeleton with surface changed aluminum (oxidized) and catalytic active nickel centers regularly distributed in this matrix. The PXRD and ^{27}Al MAS NMR experiments could detect the oxidation of Al during sonication. Our previous works[25] on ultrasound treatment of aluminum and nickel particles demonstrate that aluminum exhibits increase of surface area and formation of porous matrix after sonication stabilized by sonogenerated aluminum oxide. Nickel particles are relatively resistant to ultrasound irradiation and slight change in surface morphology was detected. The SEM images demonstrate formation of a rough metal oxide on the surface of the modified Ni particles. Since the concentration of NiO is very low in the system we could detect it by using XPS only. Formation of a several-nm-thick metal oxide layer plays an important role in structure stabilization without negative effect to its catalytic activity. The importance of formation of metal oxide for the structure stabilization

Adv. Funct. Mater. **2012**,
DOI: 10.1002/adfm.201200437

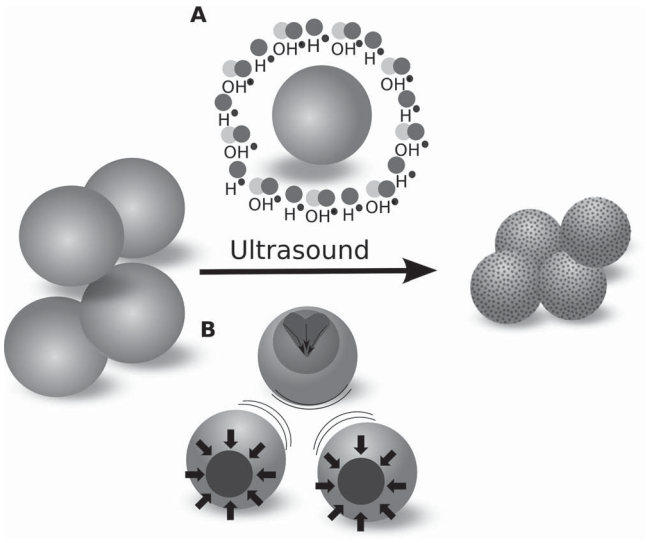

Figure 5. Sonochemical modification of metal particles: (I) initial particles; (II) chemical aspect surface oxidation (A) and physical aspects (B) interparticle collisions; (III) formation of mesoporous metals.

during sonication can be proved by the addition experiments in an inert solvent. It has been suggested that in IL the oxidation could be avoided. We performed the sonication of Al/Ni alloy in ionic liquid (IL), 1-butyl-3-methylimidazolium chloride), in order to see if the similar mesoporous structure could be formed without metal oxide stabilization. The sonication in ionic liquid did not lead to formation of porous structure. There were no other crystalline phases detected. Thus, the surface oxidation has a crucial role in stabilization of the modified metal matrix and formation of porous structure. Furthermore, the sonogenerated oxide layer provides excellent stability of the catalyst during its exploitation. The sonicated Al/Ni can be stored and used at ambient conditions in comparison to Raney nickel that is pyrophoric and requires special storage conditions.[21,22]

Thus, sonochemical modification of metal particles schematically illustrated in **Figure 5** has the following effects generated by acoustic cavitation: sonochemical one - surface redox reactions by sonogenerated free radicals (A) and sonomechanical one - interparticle collisions (B). USHI induces particle breakage and increase of surface area of the material. Simultaneously depassivation of metal surface occurs due to cavitation stimulated breakage of initial oxide layer. Then the increased metal surface is stabilized by sonogenerated oxide layer. The generation of hydrogen during sonochemical oxidation of aluminum matrix plays an important role in catalyst activation. By adjustment of the sonication process we can avoid the complete material oxidation and achieve the particle reduction of nickel particles.

2.2. Catalytic Performance

The central motivation for the investigation described here is the influence of an ultrasonic treatment on morphology, texture, and performance of a composite material. In this paper,

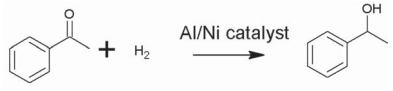

Scheme 1. Hydrogentation of acetophenone.

we tested the catalyst for the model reaction of hydrogenation of acetophenone (**Scheme 1**). As a material of interest, Al/Ni alloy powder sonicated for 50 min with maximum surface area of 125 $m^2\ g^{-1}$ was chosen. This material has previously shown its potential as catalyst.[24]

The initial Al/Ni alloy particles show no catalytic activity in the hydrogenation of acetophenone under 60 bar H_2-pressure and stirring at room temperature (RT) and water as a solvent. No or poor catalytic activity for commercially available and untreated Al/Ni alloys have also been reported.[50,51] On a contrary the sonochemically activated Al/Ni material demonstrates catalytic activity. It is important, that there were no side products observed during the hydrogenation of acetophenone under the used condition (RT, 60 bar of H_2). The catalytic experiments are summarized in **Table 1**.

The conversion of acetophenone to 1-phenylethanol was measured after 24 hours of reaction by gas chromatography (GC). The optimal conversion (>99.9%) of acetophenone was observed when 50 mg of catalyst were used (Table 1, Entry 1-2).

The pressure of the hydrogen applied during the catalytic reaction has its crucial influence on the conversion of acetophenone to 1-phenylethanol (Table 1, Entry 2-5). To avoid diffusion limitation we have chosen a pressure of 60 bar as the standard condition. It was observed that the yield of 1-phenylethanol decreases when the pressure is reduced. The maximum yield of 1-phenylethanol was observed at a hydrogen pressure of 40 bar, 5 bar hydrogen pressure gave a yield of 34%.

Using the optimal conditions of 50 mg of Al/Ni catalyst and a hydrogen pressure of 60 bar the conversion was studied based on the reaction time. Therefore, several catalytic runs were performed and stopped after a specific period of time. The complete consumption of the applied acetophenone was observed after the reaction time of 4 hours.

In addition the Al/Ni catalyst was tested under standard conditions (RT, 60 bar H_2, water as the solvent, 50 mg Al/Ni

Table 1. Conversion of acetophenone in dependence of H_2-pressure, amount of catalyst, as well as amount of substrate for a reaction time of 24 h at RT, stirring and 1 mL water as a solvent.

Entry	Catalyst [mg]	Acetophenone [µL]	H_2-pressure (bar)	Conversion of acetophenone [%]
1	25	300	60	36
2	50	300	60	> 99.9
3	50	300	5	34
4	50	300	20	79
5	50	300	40	> 99.9
6	50	500	60	> 99.9
7	50	700	60	> 99.9
8	50	900	60	> 99.9
9	50	1100	60	> 99.9

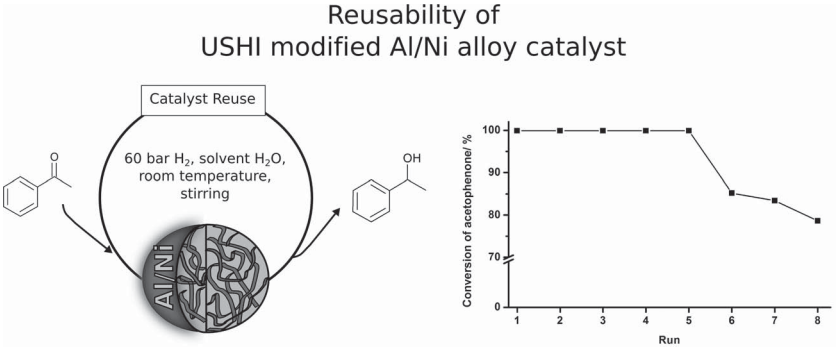

Figure 6. Reusability of Al/Ni catalyst under standard condition, namely 50 mg of USHI modified Al/Ni catalyst, 1 mL water as a solvent, reaction time 6 h at room temperature under 60 bar H_2 and stirring.

catalyst, stirring, 24 h reaction time) with higher amounts of acetophenone, namely 300 mL up to 1.1 mL (9.57 mmol). One could see that performance of the catalyst has not changed (Table 1, Entry 2 and 6-9).

To investigate the catalyst reusability, we performed catalytic reactions under the conditions described above and the reaction time of 6 hours (**Figure 6**). It was found that under these conditions the catalyst produces >99.9% 1-phenylethanol within the first five runs. After 5 runs the yield slightly decreased upon reuse, but still remained effective after 8 runs. The consumption of the acetophenone is gone down to 78% after 8 runs.

The unique morphology of our sonoactivated Al/Ni system (presence of metallic Ni and sonogenerated metal oxides) provides easy and efficient catalytic performance of the material. First of all the catalyst does not require preactivatetion stage before use. If the catalyst was preactivated for 24 h in a hydrogen atmosphere (solid catalyst material) no increase in catalytic activity was observed. Then, the sonoactivated Al/Ni can be a good alternative to the commercial Raney nickel. The activity of sonochemically activated Al/Ni was compared with the commercial Raney Ni catalyst. Similar activities were observed, conversion of acetophenone to 1-phenylethanol (60 bar H_2 pressure) at room temperature, for our best catalyst and commercial Raney nickel catalyst.

3. Conclusions

The sonochemical activation of Al/Ni particles results in nanostructuring of initial Al/Ni alloy and formation of an effective catalyst for the hydrogenation of acetophenone. The novel formation/activation method is based on the cavitation induced mechanochemical particle breakage and metal depassivation (breakage of initial oxide layer). The structure stabilisation is achieved by sonochemical formation of surface metal oxide layer. The self-regulated nickel reduction process (also in porous matrix of the catalyst) is responsible for formation of active centres of the catalysts. Thus, upon sonochemical activation the alloy species adopt a number of features attractive for catalytic applications: high surface area (up to 125 $m^2\ g^{-1}$) and narrow pore size (~4 nm) distribution, presence of metallic nickel. In addition, the easy storage and handling of the metal based stabilized by thin oxide layer Al/Ni catalyst is an advantage of our system. The ability to reuse the catalyst with little or no decrease of product yield makes the procedure of ultrasound activation for catalyst formation an attractive alternative to other preparation methods. Thus, the sonochemically activated Al/Ni alloy could become a great alternative to known Raney nickel[20] and other heterogeneous hydrogenation catalysts. The findings presented here provide guidelines for the extension of the concept towards a broad variety of systems.

4. Experimental Section

Materials: Aluminum-nickel alloy powder (Fluka) (composition: 50 wt% aluminum and 50 wt% nickel) was used with a particle size ca. 100 µm as received. The water was purified before use in a three stage Millipore Milli-Q Plus 185 purification system and had a resistivity higher than 18.2 MΩ ·cm.

Preparation of Al/Ni catalyst: 5 g of the commercial Al/Ni alloy were dispersed in purified water (50 mL) and sonicated up to 50 min with an ultrasound tip (VIP1000hd, Hielscher Ultrasonics GmbH, Germany) operated at 20 kHz with a maximum output power of 1000 W ultrasonic horn BS2d22 (head area of 3.8 cm^2) and equipped with a booster B2-1.8. The maximum intensity was calculated to be 140 W cm^{-2} at mechanical amplitude of 106 µm. To avoid the temperature increase during sonication the experiment was performed in a thermostatic cell. After the USHI treatment, the sample was dried under vacuum with a heat gun.

Scanning electron microscopy: Scanning electron microscopy (LEO 1530 FE-SEM, Zeiss) was applied to characterize the optical response, structure, and size of the nanoparticles.

Powder X-ray diffraction: Powder X-ray diffraction (PXRD) diagrams were collected at θ–θ mode using a Stoe STADI P X-ray Transmission diffractometer: Cu Kα_1, irradiation, room temperature, $2*\theta = 5$–90.

^{27}Al MAS NMR: The *^{27}Al MAS NMR* spectra were recorded at room temperature with a Bruker Avance II 300 FT NMR spectrometer operating at 78.2 MHz for ^{27}Al. The samples were loaded into 2.5 mm ZrO_2 rotors and mounted in a commercial triple resonance MAS probe (Bruker). All spectra were collected using proton broadband decoupling with a spinal64 sequence and a nutation frequency of 70 kHz. The recycle delay and spinning speed were adjusted to 1 s and 30 kHz. To eliminate not desirable signals from the probe we applied a rotor-synchronized Hahn echo sequence with a 16 step phase cycle and a nutation frequency of 50 kHz. The first and second pulse of the echo were set to 1 µs and 2 µs, respectively, to ensure that the signal intensity becomes independent from the magnitude of the quadrupolar coupling. The chemical shift of the ^{27}Al resonance is given with respect to $[Al(H_2O)_6]^{3+}$. The simulations of the MAS spectra were carried out with the program package SIMPSON.[52]

Surface area and pore size distribution: Surface area and pore size distribution based on physisorption (adsorption and desorption of gases) were measured by the BET (Brunauer-Emmett-Teller)[43] and BJH (Barrett-Joyner-Halenda)[42] method using N_2 at 77 K on a vacuum gas sorption NOVA 2000e (Quantachrome). The samples were dried under vacuum for 24 h at 300 °C.

Pulse Titration Analysis: Pulse Titration Analysis was performed by CHEMBET Pulsar TPD/TPR (Quantachrome) with hydrogen as the titration gas at a temperature of 300 K. Five hydrogen impulses were applied with a flow rate of 75 $cm^3\ min^{-1}$ at an ambient pressure of 760.00 mmHg.

Inductively Coupled Plasma (ICP): Inductively Coupled Plasma by Perkin Elmer, Plasma 400 with Argon Plasma determined the nickel content.

DOI: 10.1002/adfm.201200437

X-ray Photoelectron Spectroscopy (XPS): XPS spectra were acquired with a SPECS hemispherical energy analyzer (Phoibus 100) and SPECS focus 500 X-Ray monochromator using the Al Kα with energy of 1486.74 eV.

Confocal Scanning Fluorescence Microscopy *(CSFM)*: A Leica TCS SP confocal laser scanning microscope (Leica, Germany) with a 100× oil immersion objective, numerical aperture 1.4 was used. The particles were loaded with a water-soluble fluorescent dye, Fluorescein. The pores of the particles were closed by the procedure suggested in.[53–56]

Catalytic application of the modified Al/Ni material: The hydrogenation of ketones was studied as described in Ref. [58,59]. The hydrogenation experiments were carried out using a Parr Instrument stainless steel autoclave N-MT5 300 mL equipped with heating mantle and temperature controller. Gas chromotography (GC) analyses were performed on an Agilent 6890 N Network GC System using a Lipodex E column (25 m × 0.25 mm; Machery & Nagel). We placed 0.05 g of the catalyst and 1 mL water in a glass vial. Additionally acetophenone (300 µL, 0.31 g, 2.57 mmol) was transferred via sealed Fortuna-Pipette. The filled vial was put into the autoclave. Subsequently, the autoclave was purged three times with hydrogen. The reduction was carried out at room temperature under vigorous stirring by using a continuous pressure of 60 bar of hydrogen. The experiment was stopped after the hydrogen gas was released. The reaction mixture was worked up by the addition of dodecane (584 µL, 0.44 g, 2.57 mmol) as internal standard and 2.5 mL diethyl ether. The product was extracted from the organic layer. The catalytic reactions were all carried out twice and several runs were analyzed.

Reusability: For testing the reusability of the catalyst, the reaction mixture was extracted 5 times with 2.5 mL of ether and afterwards treated in a standard ultrasound bath for 5 min. To remove the ether, the mixture was heated in 90 °C water bath for 10 minutes. After that, the Al/Ni catalyst was used again for the hydrogenation under standard conditions.

Supporting Information

Supporting Information is available from the Wiley Online Library or from the author.

Acknowledgements

This work was supported by SFB840. We are grateful to Bernd Putz (Bayreuth University) for carrying out the PXRD as well as to Lena Geiling (Bayreuth University) for BET measurements. E. V. S. thanks to Alexander von Humboldt Foundation.

Received: February 12, 2012
Revised: March 26, 2012
Published online:

[1] R. Karmhag, T. Tesfamichael, E. Wackelgard, A. Niklasson, M. Nygren, *Sol. Energy* **2000**, *68*, 329.
[2] T. Hyeon, *Chem. Commun.* **2003**, 927.
[3] K. Kim, S. C. Jeoung, J. Lee, T. Hyeon, J. I. Jin, *Macromol. Symp.* **2003**, *201*, 119.
[4] I. S. Lee, N. Lee, J. Park, B. H. Kim, Y. W. Yi, T. Kim, T. K. Kim, I. H. Lee, S. R. Paik, T. Hyeon, *J. Am. Chem. Soc.* **2006**, *128*, 10658.
[5] W. J. Tseng, C. N. Chen, *J. Mater. Sci.* **2006**, *41*, 1213.
[6] A. Houdayer, R. Schneider, D. Billaud, J. Ghanbaja, J. Lambert, *Synthetic Met.* **2005**, *151*, 165.
[7] A. Saxena, A. Kumar, S. Mozumdar, *Appl. Catal. A-Gen.* **2007**, *317*, 210.
[8] J. Banhart, *Prog. Mater. Sci.* **2001**, *46*, 559.
[9] J. Erlebacher, M. J. Aziz, A. Karma, N. Dimitrov, K. Sieradzki, *Nature* **2001**, *410*, 450.
[10] Y. Ding, J. Erlebacher, *J. Am. Chem. Soc.* **2003**, *125*, 7772.
[11] M. Raney, *USA Patent*, *US1563587*, **1925**.
[12] H. M. Luo, L. Sun, Y. F. Lu, Y. S. Yan, *Langmuir* **2004**, *20*, 10218.
[13] Y. Yamauchi, T. Momma, T. Yokoshima, K. Kuroda, T. Osaka, *J. Mater. Chem.* **2005**, *15*, 1987.
[14] A. Devasenapathi, H. W. Ng, C. M. S. Yu, S. W. Lim, *J. Mater. Sci.* **2005**, *40*, 5463.
[15] G. S. Attard, P. N. Bartlett, N. R. B. Coleman, J. M. Elliott, J. R. Owen, J. H. Wang, *Science* **1997**, *278*, 838.
[16] O. D. Velev, P. M. Tessier, A. M. Lenhoff, E. W. Kaler, *Nature* **1999**, *401*, 548.
[17] H. Maeda, Y. Kusunose, M. Terasaki, Y. Ito, C. Fujimoto, R. Fujii, T. Nakanishi, *Chem-Asian J* **2007**, *2*, 350.
[18] H. Masuda, K. Fukuda, *Science* **1995**, *268*, 1466.
[19] H. J. Shin, C. H. Ko, R. Ryoo, *J. Mater. Chem.* **2001**, *11*, 260.
[20] M. Raney, *Ind. Eng. Chem.* **1940**, *32*, 1199.
[21] J. Masson, P. Cividino, J. Court, *Appl. Catal. A-Gen.* **1997**, *161*, 191.
[22] P. Mars, T. V. D. Mond, J. J. Scholten, *Ind. Eng. Chem. Prod. Rd.* **1962**, *1*, 161.
[23] E. V. Skorb, D. G. Shchukin, H. Möhwald, D. V. Andreeva, *Nanoscale* **2010**, *2*, 722.
[24] E. V. Skorb, H. Möhwald, T. Irrgang, A. Fery, D. V. Andreeva, *Chem. Commun.* **2010**, *46*, 7897.
[25] E. V. Skorb, D. Fix, D. G. Shchukin, H. Möhwald, D. V. Sviridov, R. Mousa, N. Wanderka, J. Schäferhans, N. Pazos-Pérez, A. Fery, D. V. Andreeva, *Nanoscale* **2011**, *3*, 985.
[26] J. Schäferhans, S. Gomez-Quero, D. V. Andreeva, G. Rothenberg, *Chem.-Eur. J.* **2011**, *17*, 12254.
[27] N. Pazos-Perez, J. Schäferhans, E. V. Skorb, A. Fery, D. V. Andreeva, *Micropor. Mesopor. Mat.* **2012**, *154*, 164.
[28] N. Pazos-Perez, T. Borke, D. V. Andreeva, R. A. Alvarez-Puebla, *Nanoscale* **2011**, *3*, 3265.
[29] J. P. Lorimer, T. J. Mason, *Chem. Soc. Rev.* **1987**, *16*, 239.
[30] K. S. Suslick, G. J. Price, *Annu. Rev. Mater. Sci.* **1999**, *29*, 295.
[31] T. Prozorov, R. Prozorov, K. S. Suslick, *J. Am. Chem. Soc.* **2004**, *126*, 13890.
[32] J. H. Bang, K. S. Suslick, *Adv. Mater.* **2010**, *22*, 1039.
[33] G. Cravotto, P. Cintas, *Angew. Chem. Int. Edit.* **2007**, *46*, 5476.
[34] J. Lindley, T. J. Mason, *Chem. Soc. Rev.* **1987**, *16*, 275.
[35] K. S. Suslick, S. J. Doktycz, E. B. Flint, *Ultrasonics* **1990**, *28*, 280.
[36] S. J. Doktycz, K. S. Suslick, *Science* **1990**, *247*, 1067.
[37] J.-L. Luche, *Ultrason. Sonochem.* **1994**, *1*, S111.
[38] D. V. Andreeva, D. V. Sviridov, A. Masic, H. Möhwald, E. V. Skorb, *Small* **2012**, *6*, 1679.
[39] J. Gensel, T. Borke, N. Pazos-Perez, A. Fery, D. V. Andreeva, E. Betthausen, A. Müller, H. Möhwald, E. V. Skorb, *Adv. Mater.* **2012**, *24*, 985.
[40] E. V. Skorb, D. V. Andreeva, H. Möhwald, *Angew. Chem. Int. Ed.* **2012**, doi: 10.1002/anie.201105084.
[41] a) N. A. Tsochatzidis, P. Guiraud, A. M. Wilhelm, H. Delmas, *Chem. Eng Sci.* **2001**, *56*, 1831; b) G. I. Kuvshinov, N. V. Dezhkunov, V. I. Kuvshinov, P. P. Prokhorenko, *Inzh.-Fiz. Zh.* **1980**, *39*, 866.
[42] E. P. Barrett, L. G. Joyner, P. P. Halenda, *J. Am. Chem. Soc.* **1951**, *73*, 373.
[43] L. Brunauer, S. Deming, W. E. Deming, E. Teller, *J. Am. Chem. Soc.* **1940**, *62*, 1723.
[44] K. S. W. Sing, D. H. Everett, R. A. W. Haul, L. Moscou, R. A. Pierotti, J. Rouquerol, T. Siemieniewska, *Pure Appl. Chem.* **1985**, *57*, 603.
[45] F. Rouquerol, J. Rouquerol, K. S. W. Sing, *Academic Press, London* **1999**, 467.
[46] S. J. Gregg, K. S. W. Sing, *Academic Press, London* **1982**, 303.

[47] B. Zeifert, J. S. Blasquez, J. G. C. Moreno, H. A. Calderon, *Rev. Adv. Mater. Sci.* **2008**, *18*, 633.
[48] S. R. Kirumakki, B. G. Shpeizer, G. V. Sagar, K. V. R. Chary, A. Clearfield, *J. Catal.* **2006**, *242*, 319.
[49] J. Jun, M. Dhayal, J. H. Shin, Y. H. Han, N. Getoff, *Appl. Surf. Sci.* **2008**, *254*, 4557.
[50] J. Petro, L. Hegedus, I. E. Sajo, *Appl. Catal. A-Gen.* **2006**, *308*, 50.
[51] F. Alonso, P. Riente, J. A. Sirvent, M. Yus, *Appl. Catal. A-Gen.* **2010**, *378*, 42.
[52] M. Bak, J. T. Rasmussen, N. C. Nielsen, *J. Magn. Reson.* **2000**, *147*, 296.
[53] R. B. Grubbs, *J. Polym. Sci., Part A: Polym. Chem.* **2005**, *43*, 4323.
[54] E. V. Skorb, D. Fix, D. V. Andreeva, H. Möhwald, D. G. Shchukin, *Adv. Funct. Mater.* **2009**, *19*, 2373.
[55] E. V. Skorb, D. V. Sviridov, H. Möhwald, D. G. Shchukin, *Chem. Commun.* **2009**, 6041.
[56] E. V. Skorb, A. G. Skirtach, D. V. Sviridov, D. G. Shchukin, H. Möhwald, *ACS Nano* **2009**, *3*, 1753.
[57] E. V. Skorb, D. G. Shchukin, H. Möhwald, D. V. Sviridov, *J. Mater. Chem.* **2009**, *19*, 4931.
[58] Y. Mei, G. Sharma, Y. Lu, M. Ballauff, M. Drechsler, T. Irrgang, R. Kempe, *Langmuir* **2005**, *21*, 12229.
[59] G. Sharma, Y. Mei, Y. Lu, M. Ballauff, T. Irrgang, S. Proch, R. Kempe, *J. Catal.* **2007**, *246*, 10.

Adv. Funct. Mater. **2012**,
DOI: 10.1002/adfm.201200437